PCCP

Accepted Manuscript

ROYAL SOCIETY OF CHEMISTRY

www.rsc.org/pccp

The Effect of Gd on trityl-based Dynamic Nuclear Polarisation in Solids

Enrico Ravera[1‡], Daphna Shimon[2‡], Akiva Feintuch[2], Daniella Goldfarb[2], Shimon Vega[2], Alessandra Flori,[3] Claudio Luchinat,[1] Luca Menichetti,[4] Giacomo Parigi[1*]

‡ Equal contribution

[1]Magnetic Resonance Center (CERM) and Department of Chemistry "Ugo Schiff", University of Florence, Italy

[2]Chemical Physics Department, Weizmann Institute of Science, Rehovot, Israel

[3]Institute of Life Sciences, Scuola Superiore Sant'Anna, Pisa, Italy

[4]Fondazione CNR/Regione Toscana G. Monasterio and Institute of Clinical Physiology, National Council of Research, Pisa, Italy

*Corresponding author: Prof. Giacomo Parigi, parigi@cerm.unifi.it

Abstract

In dynamic nuclear polarization (DNP) experiments performed under static conditions at 1.4 K we show that the presence of 1 mM Gd(III)-DOTAREM increases the ^{13}C polarization and decreases the ^{13}C polarization buildup time of ^{13}C-urea dissolved in samples containing water/DMSO mixtures with trityl radical (OX063) concentrations of 10 mM or higher. To account for these observations further measurements were carried out at 6.5 K, using a combined EPR and NMR spectrometer. At this temperature, frequency swept DNP spectra of samples with 5 or 10 mM OX063 were measured, with and without 1 mM Gd-DOTA, and again a ^{13}C enhancement gain was observed due to the presence of Gd-DOTA. These measurements were complemented by electron-electron double resonance (ELDOR) measurements to quantitate the effect of the electron spectral diffusion (eSD) and its effect on the DNP enhancements and lineshapes. Simulations of the ELDOR spectra were done using the following parameters: i) a parameter defining the rate of the eSD process, ii) an “effective electron-proton anisotropic hyperfine interaction parameter”, and iii) the transverse electron spin relaxation time of OX063. These parameters, together with the longitudinal electron spin relaxation time, measured by EPR, were used to calculate the frequency profile of the electron polarization. This, in turn, was used to calculate two basic solid effect (SE) and indirect cross effect (iCE) DNP spectra. A properly weighted combination of these two normalized DNP spectra provided a very good fit of the experimental DNP spectra. The best fit simulation parameters reveal that the addition of Gd(III)-DOTA causes an increase in both

the SE and the iCE contributions by similar amounts, and that the increase in the overall DNP enhancements is a result of narrowing of the ELDOR spectra (increased electron polarization gradient across the EPR line). These changes in the electron depolarization profile are a combined result of shortening of the longitudinal and transverse electron spin relaxation times, as well as an increase in the eSD rate and in the effective electron-proton anisotropic hyperfine interaction parameter.

Introduction

In Dynamic Nuclear Polarization (DNP) the electron spin Boltzmann population distribution of a paramagnetic center is transferred to the neighboring nuclei *via* the irradiation with a microwave (MW) field, yielding significant enhancement of the NMR signal. DNP was theorized by Overhauser in 1953,[1] and then brilliantly demonstrated by Carver and Slichter shortly after.[2] In the last decade, DNP has regained interest within the NMR and MRI communities thanks to the methodological breakthroughs, the introduction of high power MW sources and further hardware developments, the synthesis of optimized paramagnetic centers as a source of polarization, and progress in sample optimization. Among the most significant developments of the past few years are the incorporation of magic angle spinning NMR to DNP and the introduction of dissolution DNP.[3-6] Dissolution DNP has gained importance for its applications in high-resolution NMR and also for imaging using hyperpolarized metabolic substrates.[7-13] In the quest for improved sample preparation conditions, several groups have shown that the use of Gd dopants, such as those commonly used as contrast agents for MRI, increase the overall enhancement gained from DNP at liquid-helium temperature in static solid samples.[14-17] However, at 240 GHz the addition of Gd caused a decrease in enhancement.[18] The mechanism that leads to this increase at 95 GHz, but to a decrease at 240 GHz, is still an open question.

Dissolution DNP experiments are performed by polarization of the sample, usually at ~3.5 T and very low temperatures (below 4 K), and then fast heating and dissolution of the sample in order to observe the liquid-state NMR spectra at higher magnetic fields (>6 T). This method takes advantage of the large DNP enhancements achievable in the solid state at very low temperatures along with the large thermal polarization at these temperatures.[4] Dissolution DNP experiments are commonly performed using the available commercial instrument HyperSense (Oxford Instruments, UK), where ^{13}C polarization is achieved at 3.35 T and 1.4 K.[4]

DNP of samples that are dielectric solids can be explained in terms of four mechanisms: Solid Effect (SE),[19] Cross Effect (CE),[20] Thermal Mixing (TM)[21-23] and Overhauser Effect (OE).[1] The first two are mostly encountered under the experimental conditions currently used in MAS-DNP and dissolution DNP,[24-34] whereas the OE has been recently observed in MAS-DNP at higher magnetic fields.[35]

The SE-DNP mechanism relies on MW irradiation at electron-nuclear zero quantum (ZQ) and double quantum (DQ) "forbidden" transition frequencies for polarization transfer from the electrons to coupled nuclei. These transitions become allowed due to the mixing of the nuclear and electron spin states caused by the presence of anisotropic hyperfine coupling, which is mainly dipolar in origin.

The CE-DNP enhancement mechanism relies on the presence of nuclei coupled to a pair of interacting electrons, with resonance frequencies ω_{S1} and ω_{S2} separated by the nuclear Larmor frequency ω_n. In a recent publication the quantum mechanics underlying the CE mechanism has been re-examined and a distinction has been made between the direct (dCE) and indirect (iCE) cross effect.[36] In particular, it was shown analytically that the dCE and iCE mechanisms arise from MW irradiation that either directly saturates one of the transitions of the CE electron pairs (dCE-DNP) or saturates the transitions of other electrons which then indirectly depolarize the CE electron pairs (iCE-DNP) via electron spectral diffusion (eSD). In the same paper it was also shown that at steady state conditions the dCE mechanism becomes part of the iCE mechanism and that the two mechanisms can differ in their buildup dynamics.

TM is a thermodynamic description of DNP, with an electron spin bath that is cooled by MW irradiation, and a nuclear spin bath that is cooled by contact with the electron spin bath.[29;37]

Generally, the DNP spectrum, i.e. the NMR enhancement as a function of the MW frequency, is a good marker for the underlying DNP mechanism as each mechanism should result in a particular lineshape.

In this manuscript we explore experimentally and theoretically the observed improvement in the DNP enhancement due to Gd(III) at 95 GHz. Relying on the iCE-DNP mechanism[36;38] and the nuclear spin diffusion mechanism[34;39;40] we provide an easy-to-understand picture of the ongoing phenomena. We show an increase in the urea ^{13}C-signal and a shortening of the electron spin-lattice relaxation time, T_{1e}, when adding Gd(III). We then show that shortening T_{1e} i) decreases the overall electron depolarization and ii) increases the polarization gradient across the EPR line and consequently causes an increase of the nuclear polarization.

Experimental Methods and Simulations

Sample preparation. All samples were prepared by dissolving 6 M ^{13}C-urea in a DMSO/H_2O 50/50 v/v mixture. The trityl radical OX063 (Oxford Instr. Ltd, Abingdon, UK) was added to the solution with concentrations ranging from 2.5 to 30 mM, with or without 1 mM Gd-DOTAREM (1,4,7,10-tetraazacyclododecane-1,4,7,10-tetraacetic acid Guerbert, Roissy CdG Cedex, France).

Samples with OX063 concentrations of 5 and 10 mM were prepared according to Ref. [25], also by dissolving the appropriate amount of OX063 and 6 M ^{13}C-urea in a DMSO/H_2O 50/50 v/v mixture. In order to get 1.1 mM Gd-DOTA, 1.1 mM of $GdCl_3$ (Sigma Aldrich, Israel) was added to the solutions, along with a slight excess of DOTA (Macrocyclics, U.S.A.).

DNP experiments – 1.4K. The buildup time constants and the maximum polarization values of the urea ^{13}C nuclei were measured with the HyperSense instrument (Oxford Instr., UK) for samples with OX063 concentration of 2.5, 5, 7.5, 10, 15 and 30 mM, by polarizing at 3.35 T and 1.4 K for about 50 minutes. The build-up curves were obtained by acquiring signals every 200 s, using a 5° flip-angle. The buildup curves were fitted to estimate the buildup time constants and plateau values. In order to compare the DNP effect in the different samples, the value of the build-up plateau was rescaled according to the number of ^{13}C nuclei present in the sample. These experiments were performed with a MW power of 85 mW.

Electron relaxation times, ELDOR experiments and DNP experiments – 6.5K.

In this work we refer to all irradiation and Larmor frequencies with respect to a reference frequency, ν_{ref}=94.86 GHz, such that instead of ν_{ξ}, we will refer to $\delta\nu_{\xi} = \nu_{\xi} - \nu_{\mathrm{ref}}$.

Electron relaxation times, T_{1e}, ELDOR and DNP measurements were performed on the four samples with OX063 concentration of 5 or 10 mM, with and without Gd-DOTA using the combined EPR and NMR spectrometer described in Ref. [41]. All measurements were conducted at 6.5 K. The MW irradiation strength was measured by nutation experiments and found to be ~600 kHz in all cases.

T_{1e} values were determined by saturation recovery experiments at the frequency of the maximum of the EPR spectrum, $\delta\nu_{MW}$=6 MHz. The electron signal was detected using an α-τ-α echo detection scheme with α pulse lengths of 400 nsec, τ=600 nsec and a saturation pulse of 50 msec.

ELDOR spectra were collected by irradiating for a time t_{MW}=1 sec at a frequency $\delta\nu_{excite}$ followed by an EPR echo detection at a frequency $\delta\nu_{detect}$. At each $\delta\nu_{detect}$ the MW frequency $\delta\nu_{excite}$ was swept over a total range of ~400MHz around the EPR line. The echo signals were then normalized with respect to echo signals detected after MW irradiation at a frequency significantly removed from the EPR line. ELDOR spectra were collected at five different $\delta\nu_{detect}$ frequencies ($\delta\nu_{detect}$=-32, -16, 0, 16 and 32 MHz, marked with black arrows in Fig. S1). The electron signal was detected using an α-τ-α echo detection scheme at $\delta\nu_{detect}$ with α pulse lengths of 450 nsec and τ =1000 nsec.

The ^{13}C buildup time constants were determined by measuring the ^{13}C signal as a function of the MW irradiation time.

The DNP spectra were acquired from 94.65 GHz to 95.06 GHz, in steps of 10 MHz with 200 sec of irradiation at each MW frequency. For these measurements FID nuclear detection was used, with a 90° pulse length of 16 µsec.

The ^{13}C thermal equilibrium signal was not measured in this work due to low ^{13}C sensitivity without DNP and long relaxation times making signal averaging unfeasible. As such we will not discuss enhancement, but only relative signal intensities between the four samples.

The derivation of the DNP lineshapes. This study is aimed at understanding the source of the increased nuclear enhancement due to the addition of Gd-DOTA to the samples. The main tool for this investigation is the analysis of the frequency swept DNP spectra of the four samples (5 mM and 10 mM) with and without Gd-DOTA. In its present form this analysis does not predict absolute values of the bulk polarization but rather provides information about changes in their values.

In the following we present a brief summary of the theory we use for the analysis of the DNP spectra derived in a recent publication. The lineshapes of the DNP spectra can be calculated from the electron polarization profiles $P_e(\delta\nu_{detect};\delta\nu_{excite})$ along the EPR spectrum, as a function of $\delta\nu_{detect}$, during MW irradiation at a given frequency $\delta\nu_{excite}$. As was previously shown[24;36;38] these $P_e(\delta\nu_{detect};\delta\nu_{excite})$ profiles can be derived using best fit parameters determined by simulations of ELDOR spectra using the solution of a rate equation model describing the polarizations of the electrons in frequency bins and a single nucleus representing the bulk nucleus in the sample under the ELDOR conditions.

In this model the electrons generating the EPR line are divided into a fixed number of frequency bins *j* (electron spin packets) with average frequencies $\delta\nu_{e,j}$ and a width Δ_{bin}, each containing a relative number f_j of electrons with polarizations $P_e(\nu_j)$. The normalized EPR lineshape defines the f_j coefficients. The dynamics of the polarization of each bin depend on T_{1e}, the spin-spin relaxation time T_{2e}, the magnitude of the MW irradiation, ω_1, and the electron spectral diffusion (eSD) process, defined by exchange rates $\overline{w}_{j,j'}^{eDS}$ derived from a *eSD* strength parameter Λ^{eSD} as follows:

$$\overline{w}_{j,j'}^{eSD} = \frac{\Lambda^{eSD}}{(\delta\nu_j - \delta\nu_{j'})^2 (2\pi)^2} \qquad (1).$$

Using this expression it is possible to derive a time constant, $T_{\max}^{eSD}$, that describes the time it takes for two neighboring bins, $j_{\max}$ and $j_{\max-1}$, at the maximum of the EPR line to equalize their polarizations. This time constant is of the form

$$T_{\max}^{eSD} = \frac{1}{\Lambda^{eSD}} \frac{2(\delta\nu_{j_{\max}} - \delta\nu_{j_{\max-1}})^2 (2\pi)^2}{(f_{\max} - f_{\max-1})^2} \qquad (2)$$

and provides us with a parameter that expresses the timescale of the eSD process corresponding to any fitting parameter Λ^{eSD} and makes it possible to compare this timescale with the other time scales of the system.

The influence of the protons on the electron polarizations is taken into account by adding to the rate equations the effect of the irradiation on the electron-proton ZQ/DQ transition (the proton SE) in the form of a proton-electron exchange rate that is proportional to an effective pseudo-hyperfine interaction parameter $\overline{A}^{\pm}$ representing the overall coupling between the electrons and the protons. The relative concentrations of the electrons and protons are also taken into account.[31] Thus in this model the free parameters determining the $P_e(\delta\nu_j)$'s and the $P_e(\delta\nu_{detect};\delta\nu_{excite})$ profiles are T_{2e}, $\overline{A}^{\pm}$ and Λ^{eSD}, while all other parameters are derived from the EPR line shape or measured experimentally. It is important to note that the $P_e(\delta\nu_{detect};\delta\nu_{excite})$ profiles are derived without relying on the TM formalism. Thus, there is no need to introduce electron spin-temperature coefficients.

As was explicitly shown in Ref. [36], and demonstrated in Ref. [24], the $P_e(\delta\nu_{detect};\delta\nu_{excite})$ profiles can be used to calculate the basic SE-DNP, $S_{SE}(\delta\nu_{MW})$, and iCE-DNP, $S_{iCE}(\delta\nu_{MW})$, lineshapes. The steady state DNP spectra can then be expressed as

$$E_{13C}(\delta\nu_{MW}) = k_{SE}S_{SE}(\delta\nu_{MW}) + k_{iCE}(S_{iCE}(\delta\nu_{MW}) - S_{iCE,0}) + c_{eq}, \qquad (3)$$

where the k coefficients, k_{SE} and k_{iCE}, express the relative contributions of the two mechanisms, c_{eq} is added to account for the thermal equilibrium value and the reason for the subtraction of the thermal equilibrium value $S_{iCE,0}$ from the iCE contribution is explained in Ref. [36]. As in our previous work,[24;36] we do not take into account the dCE lineshape, as at steady state the electrons polarized by the dCE are included in the iCE calculation.

The basic iCE-DNP spectrum, $S_{iCE}(\delta\nu_{MW})$ is calculated by taking into account all CE electron pairs, with Larmor frequencies of $\delta\nu_e$ and $\delta\nu_e - \delta\nu_C$, where $\delta\nu_C$ is the ^{13}C Larmor frequency, and their polarization differences $P_e(\delta\nu_e;\delta\nu_{MW}) - P_e(\delta\nu_e - \delta\nu_C;\delta\nu_{MW})$. The relative number of these electron pairs $f(\delta\nu_e)\times f_e(\delta\nu_e - \delta\nu_n)$ is also included into the calculation, such that the overall expression is:

$$S_{iCE}(\omega_{MW}) = N_{iCE}^{-1}\int d\delta\nu_e\ f(\delta\nu_e)\times f(\delta\nu_e - \delta\nu_C)\frac{P_e(\delta\nu_e;\delta\nu_{MW}) - P_e(\delta\nu_e - \delta\nu_C;\delta\nu_{MW})}{1 - P_e(\delta\nu_e;\delta\nu_{MW})\times P_e(\delta\nu_e - \delta\nu_C;\delta\nu_{MW})} \qquad (4)$$

where N_{iCE} is a normalization factor.

The basic SE-DNP spectrum, $S_{SE}(\delta\nu_{MW})$, can be obtained by taking into account the ZQ and DQ irradiation effects on the electron polarization, $P_e(\delta\nu_{MW} - \delta\nu_C; \delta\nu_{MW})$ and $P_e(\delta\nu_{MW} + \delta\nu_C; \delta\nu_{MW})$, and the number of electrons at $\delta\nu_{MW} \pm \delta\nu_c$, $f(\delta\nu_{MW} - \delta\nu_C)$ and $f(\delta\nu_{MW} + \delta\nu_C)$:

$$S_{SE}(\delta\nu_{MW}) = N_{SE}^{-1}\{f(\delta\nu_{MW} + \omega_C)P(\delta\nu_{MW} + \delta\nu_C; \delta\nu_{MW}) - f(\delta\nu_{MW} - \delta\nu_C)P(\delta\nu_{MW} - \delta\nu_C; \delta\nu_{MW})\}, \quad (5)$$

where N_{SE}^{-1} is a normalization factor.

Calculating these contributions to the DNP spectra and determining k_{iCE} and k_{SE} enable us to simulate the experimental DNP data (Eq. 3).

Results and discussion

Measurements at 1.4 K

Buildup curves were measured at 1.4 K for OX063 concentrations between 7.5 and 30 mM. The curves could be fitted with a monoexponential function. The ^{13}C buildup time constants and the maximum polarization achieved are reported in Fig. 1 and Table S1. As expected, the ^{13}C buildup time decreases with increasing radical concentration (Fig. 1a). In the presence of Gd-DOTAREM the buildup time of urea ^{13}C decreases by about 10-20% (see Table S1, this increase is not apparent in Fig. 1a due to the large range of the scale) for OX063 concentrations of 10-30 mM, differently from what reported for ^{13}C pyruvate. [14;15]

At variance with the high concentration cases, for OX063 concentrations of 2.5 and 5 mM, both with and without Gd-DOTAREM, the buildup curves could not be nicely fitted with a monoexponential function; in these cases, a biexponential fit was thus performed, pointing to the presence of a minor component (of about 10%) with a much shorter buildup time constant. For the sample with 2.5 mM OX063 concentration, the fast buildup time amounts to 520 s and 330 s without and with Gd-DOTAREM, respectively, whereas the slow buildup time constant is about 22000 s in both cases. As the buildup times of the observed bulk nuclei are in general of the order of, or somewhat shorter than, the nuclear T_{1n} , the short buildup components could be attributed to nuclei that are in close vicinity to the OX063 radicals. We may suggest that these very different time constants observed for very low OX063 concentrations refer to two pools of urea nuclei: the nuclei relatively far from the radical, that polarize slowly, and the nuclei closer to the radical. As the radical concentration increases, the relaxation time of the slower-relaxing pool of nuclei decreases, coming closer to the relaxation time of the faster relaxing nuclei and masking their contribution.

We may speculate that the decrease in the buildup time constant observed in the presence of Gd-DOTAREM is a result of a shortening of the longitudinal relaxation times of the ^{13}C nuclei surrounding the radicals. The latter may in turn be a result of a shortening of T_{1e} of the OX063 electrons when Gd-DOTAREM is added to the sample (see next section). In fact, a decrease of the relaxation time T_{1n}^{p} of ^{13}C nuclei of the urea molecules positioned within a few Å from the radical, referred to as core nuclei, is expected from the dipole-dipole interaction with the OX063 electron according to the relationship

$$1/T_{1n}^{p} = \frac{2}{15}\left(\frac{\mu_0}{4\pi}\right)^2 \frac{g^2\mu_B^2\gamma_{13C}^2}{r^6} S(S+1)\left[\frac{7T_{2e}}{1+\omega_e^2 T_{2e}^2} + \frac{3T_{1e}}{1+\omega_{13C}^2 T_{1e}^2}\right] \qquad (6)$$

where $1/T_{1n}^{p} = 1/T_{1n} - 1/T_{1n}^{dia}$, and T_{1n}^{dia} is the nuclear T_{1n} in the absence of paramagnetic species in solution, ω_e and ω_{13C} are the Larmor frequencies of the OX063 electron and of the ^{13}C nucleus, respectively, T_{1e} and T_{2e} are the longitudinal and transverse electron relaxation times of the radical, *S*=1/2 and *r* is the OX063-urea ^{13}C distance. For the expected values of T_{1e} and T_{2e} the above relationship may imply that a decrease in T_{1e} produces a decrease in T_{1n}^{p}. A more dramatic decrease of T_{1e} with respect to T_{1n} (see next section) upon addition of Gd(III) could be related to a small/negligible T_{1n}^{p} with respect to T_{1n}^{dia} of bulk nuclei. The decrease of T_{1e} occurring in the presence of Gd(III) could have the effect of decreasing the relaxation time of protons through their dipole-dipole interaction with the OX063 and Gd(III) radicals. On the other hand, the small change in the relaxation times of the ^{13}C nuclei of urea would then be a result of the decrease of the T_{1n} of the protons coupled to ^{13}C nuclei with short T_{1n}^{p} via the nuclear dipole-dipole interactions.[42] In the next section we will show that at 6.5 K there is indeed a decrease in T_{1e} when Gd(III) is added to 5 mM and 10 mM OX063 concentration samples. However, at this temperature, the ^{13}C buildup time, which is of the order of T_{1n} or shorter, does not change.

Presumably, this is because at these concentrations, the effect of T_{1e} on the T_{1n} of the core nuclei has a negligible effect on the bulk nuclei.

As clearly shown in Fig. 1b, and in agreement with previous experiments on pyruvate,[14;15] the urea ^{13}C polarization increases sizably in the presence of Gd-DOTAREM for OX063 concentrations of 10-30 mM. However, the polarization increases only marginally for low OX063 concentrations.

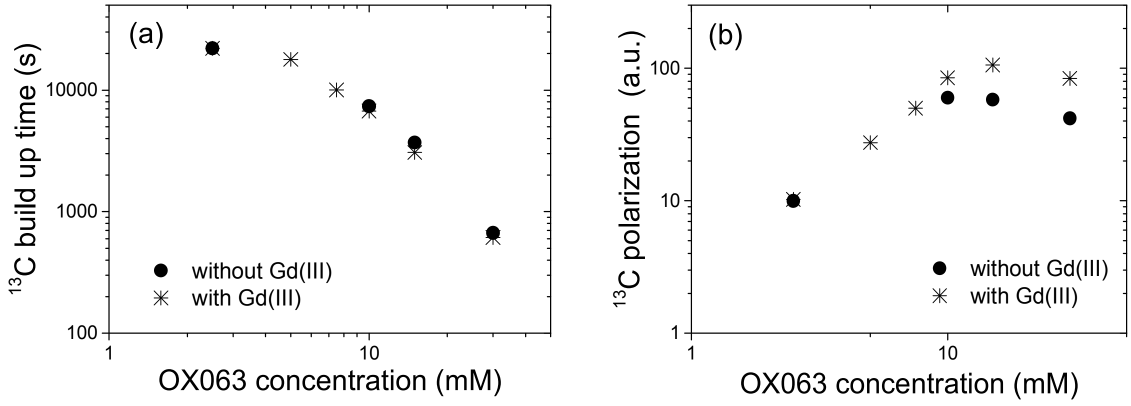

Figure 1. ^{13}C buildup time constant (a) and maximum polarization (b) measured with HyperSense (3.35 T and 1.4 K) for samples 6 M ^{13}C-urea with OX063 concentration of 2.5, 5, 7.5, 10, 15 and 30 mM, with and without 1 mM Gd-DOTA. The values at 2.5 and 5 mM refer to the major components of the bi-exponential fit (see text).

In order to rationalize the effects induced by the presence of Gd-DOTAREM on urea ^{13}C polarization, as detected at 1.4 K, a series of new experiments were performed with a combined EPR and NMR spectrometer, also allowing acquisition of T_{1e} values, ELDOR and DNP spectra under the same experimental conditions. Although these measurements were conducted at 6.5 K, we expect their DNP results to show the same trends observed at 1.4 K. This way, the DNP enhancements could be measured together with the detection of DNP spectra and their analysis using the information obtained from the ELDOR measurements. This analysis was conducted on samples with OX063 concentrations of 5 and 10 mM, with and without 1.1 mM Gd-DOTA. These two concentrations were chosen, because they were expected to represent the transition from no effect of Gd(III) addition to an increased enhancement.

ELDOR and DNP measurements at 6.5 K

^{13}C buildup measurements

Measurements of the ^{13}C buildup time constants were also performed for the four samples (5 mM and 10 mM, with and without Gd-DOTA) on the homebuilt DNP spectrometer [41]. The values were measured at 6.5 K, except for the sample with 10 mM OX063, where the temperature fluctuated between 7.5 K and 8.5 K. The time constants were determined by following the buildup of the hyperpolarization as a function of the length of the MW irradiation and fitting the data with a single exponential function that gave satisfactory fits (Table 2). The relatively large errors are due to the fact that the fittings were done by leaving the steady state values as free parameters.

The buildup time constants should reflect the length of the urea ^{13}C spin-lattice relaxation times, T_{1C}, though they can be shorter.[36;38;25;34] We note that they do not show any clear dependence on the OX063 concentration (in the 5-10 mM range) and in the presence of Gd-DOTA. The values are about 2000-3000 s, which is about 3-6 times shorter than what was measured at 1.4 K with the HyperSense. This is likely a result of the decrease in T_{1C} with increasing temperatures.

Electron spin relaxation measurements

The electron spin relaxation times of OX063 (5 mM and 10 mM) in the presence and in the absence of Gd-DOTA were measured at $\delta\nu_{MW} =$6 MHz (which is the maximum of the EPR spectrum) and at 6.5 K (see Fig. 2) through saturation recovery experiments. The curves obtained for 10 mM OX063 concentrations, and 5 mM OX063 concentration in the presence of Gd-DOTA could be fitted with a single exponential. The curve obtained for the 5 mM sample in the absence of Gd-DOTA was fitted with a double exponential. The long timescale, which is responsible for 65% of the signal recovery, is considered to be T_{1e}, and the short timescale must be related to the eSD process. In the other samples we did not observe this eSD timescale, likely because it was fully suppressed due to the long saturation pulse.

The data, summarized in Table 2, clearly show that the presence of Gd-DOTA has the effect of decreasing the magnitude of the electron relaxation time of OX063 by an order of magnitude. This decrease can be ascribed to the dipole-dipole interaction between the two types of paramagnetic centers. In fact, with the addition of the Gd-DOTA ions the electron relaxation rate of OX063 is increased according to:

$$1/T_{1e}^{+Gd} = 1/T_{1e}^{-Gd} + 1/T_{1e}^{Gd-OX063} \ , \qquad (7)$$

where $1/T_{1e}^{Gd\text{–}OX063}$ is determined by their dipolar interactions and can be derived having the form:[43]

$$1/T_{1e}^{Gd-OX063} = \left(\frac{\mu_0}{4\pi}\right)^2 \left(\frac{1}{\hbar}\right)^2 g_e^4 \mu_B^4 S_2(S_2+1) \times \sum_i r_i^{-6} \left(\frac{1}{6}(1-3\cos^2\theta_i)^2 \frac{\tau_{s2(2)}}{1+(\omega_{S1}-\omega_{S2})^2 \tau_{s2(2)}^2} \right. \qquad (8)$$
$$\left. + 3\sin^2\theta_i \cos^2\theta_i \frac{\tau_{s2(1)}}{1+\omega_{S1}^2 \tau_{s2(1)}^2} + \frac{3}{2}\sin^4\theta_i \frac{\tau_{s2(2)}}{1+(\omega_{S1}+\omega_{S2})^2 \tau_{s2(2)}^2} \right)$$

Here θ_i is the angle between the OX063–Gd(III) vector and the static magnetic field, r_i is their distance, ω_{S1} and ω_{S2} are the Larmor frequencies of OX063 and Gd(III), respectively, $\tau_{s2(i)}$ is the electronic (*i*=1, longitudinal; *i*=2, transverse) relaxation time of Gd(III) (the fast relaxing ion), and S_2 the spin quantum number of Gd(III). The parameters determining the value of $1/T_{1e}^{Gd\text{–}OX063}$, such as the r_i distance and the $\omega_{S1}-\omega_{S2}$ frequency difference, vary in the sample so that the value of $1/T_{1e}^{Gd\text{–}OX063}$ is difficult to evaluate. However, it is apparent that the source of the difference between the OX063 relaxation time in the absence (T_{1e}^{-Gd}) and in the presence (T_{1e}^{+Gd}) of Gd(III) is this dipolar interaction.

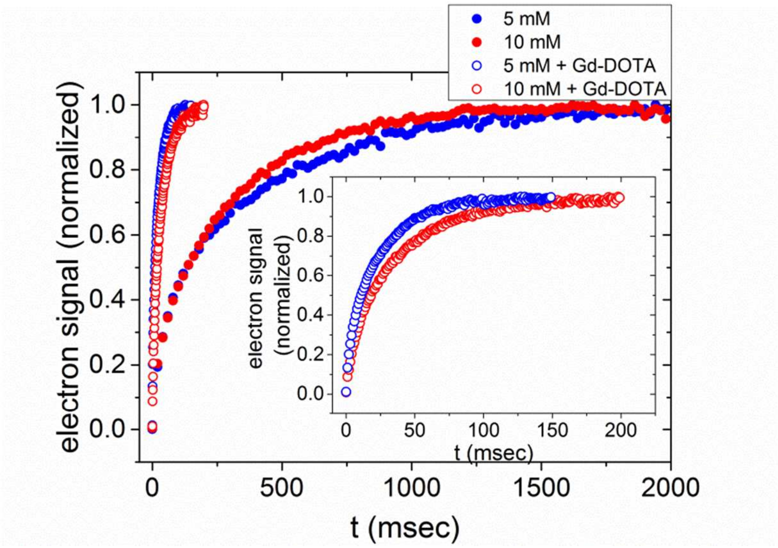

Figure 2. Electron saturation recovery curves measured for 5 mM (blue circles) and 10 mM (red circles) OX063 in the presence (open symbols) and in the absence (filled symbols) of 1 mM Gd-DOTA, at $\delta\nu_{MW} = 6$ MHz and 6.5 K. The inset shows a zoom in of the electron saturation recovery curves measured in the presence of 1 mM Gd-DOTA.

	T_{1e} (ms)	^{13}C buildup time (sec)
5 mM OX063	494±29*	2592±700
5 mM OX063 + 1mM Gd-DOTA	35±1	2962±630
10 mM OX063	317±8	2440±400**
10 mM OX063 + 1mM Gd-DOTA	24±1	2164±272

*Long timescale; **temperature between 7.5 and 8.5 K

Table 2: OX063 electron spin relaxation times and urea ^{13}C buildup time constants at 6.5 K

Measurements of DNP spectra

Fig. 3 shows the experimental frequency swept DNP spectra of the four 5 mM and 10 mM OX063 samples, with and without Gd-DOTA, measured at 6.5 K. For an easier comparison of the data the experimental spectra were rescaled such that the maximum enhancement of the 5 mM sample was set equal to 1. As a result we see that the maximum enhancement of the 5 mM sample with Gd-DOTA is about 35% higher than that of the sample without Gd-DOTA. Furthermore the 10 mM samples without and with Gd-DOTA show maxima of 2.3 and 3, respectively, again showing an increase of ~30% after the Gd-DOTA addition.

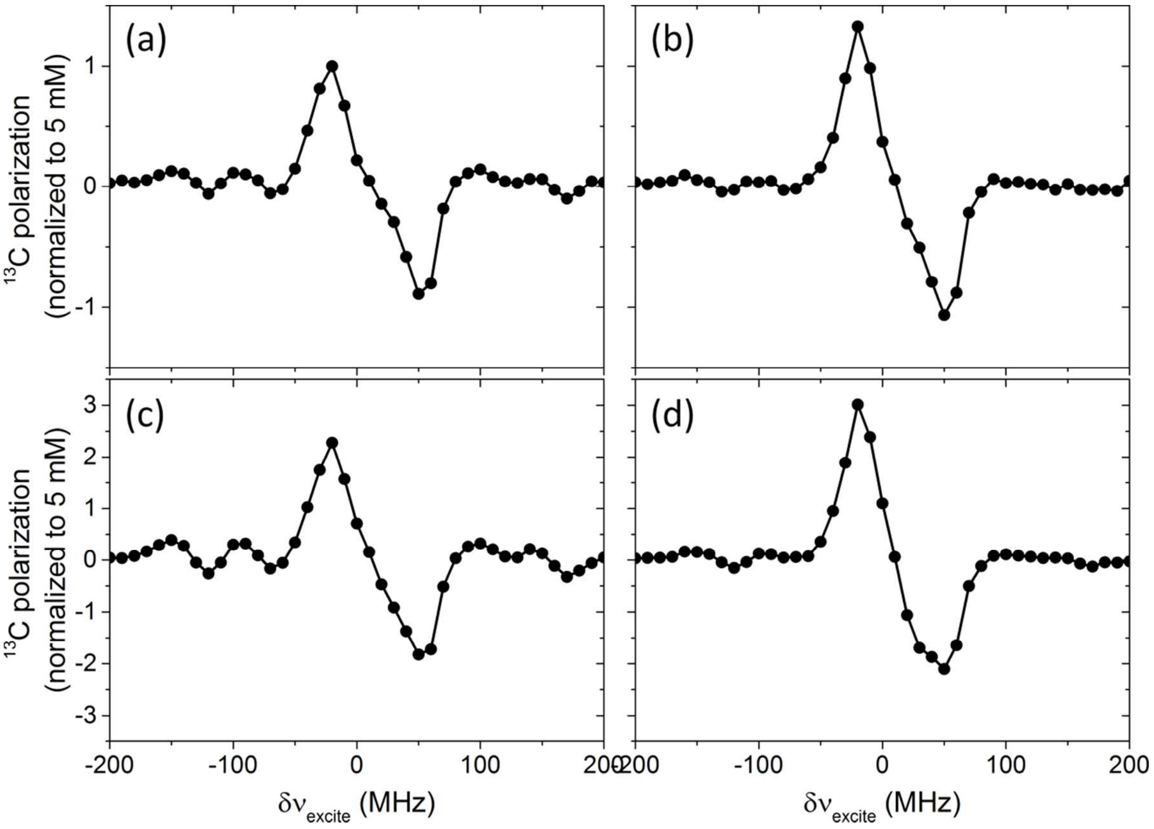

Figure 3. ^{13}C-DNP spectra measured at 6 K of the (a) 5 mM, (b) 5 mM + Gd-DOTA, (c) 10mM and (d) 10 mM + Gd-DOTA samples. The vertical axis in the figures are the ^{13}C signals measured as a function of $\delta\nu_{excite}$, where the signals are normalized with respect to the signal of the 5 mM sample (a).

ELDOR measurements

For the same samples, ELDOR spectra were recorded at five different $\delta\nu_{detect}$ values (see Experimental method section). Two of the five ELDOR profiles for each sample are shown in Fig. 4 (black symbols) and the rest in the SI.

Each ELDOR spectrum shows the depolarization of the electrons at $\delta\nu_{detect}$ when the MW irradiation is placed at $\delta\nu_{excite}$. There are three distinct regions of electron depolarization. In the middle, between -80 and 80 MHz the depolarization of the electrons at $\delta\nu_{detect}$ is due to on and off-resonance irradiation on the SQ electron transition (directly on the EPR line). On the low frequency (<-80 MHz) and high frequency (>80 MHz) sides the depolarization is due to irradiation on the electron-proton DQ and ZQ electron transitions, respectively. The overall width of the SQ, DQ and ZQ depolarizations is a mixture of both off-resonance irradiation on the detected transition and eSD which spreads the depolarization throughout the EPR line.[38]

Fig. S5 shows the superimposed ELDOR spectra at the same OX063 concentrations, with and without Gd-DOTA for better comparison. The ELDOR spectra with Gd-DOTA are clearly narrower than the ELDOR spectra without it. As such, it seems that the shortening of T_{1e} when Gd-DOTA is added also causes a narrowing of the ELDOR lines.

As can be seen the ELDOR profiles, the different sample compositions show different features that can be accounted for by analyzing these spectra using the method described in the “Experimental Methods and Simulations” section.

For each of the four samples, all five ELDOR spectra acquired were simultaneously fit with the same set of three parameters (Λ^{eSD}, $\overline{A}^{\pm}$ and T_{2e}) and the experimental echo detected EPR line of the same sample measured on a W-

Band EPR spectrometer. The longitudinal electron spin relaxation time, T_{1e}, used for the fitting was fixed according to the values reported in Table 2. Other parameters entering the model are the MW power, $\omega_1 / 2\pi = 600\, kHz$; the temperature, T=6.5 K; the irradiation time, t_{MW}=1 sec; the electron bin width, set to 2 MHz; the electron spin concentration, set to the OX063 concentration; and the proton concentration, set to 100 M. The proton polarization is expected to have a spin-lattice relaxation time, T_{1H}, that is much longer than the timescale of the ELDOR experiment, and therefore its value in the simulations does not affect the ELDOR spectra. It is not necessary to take into account the ^{13}C nuclei in the sample when calculating the ELDOR spectra, as good fits are obtained in their absence. This is consistent with previously published work on ^{13}C DNP [36] where only the ^{1}H nuclei were needed in order to fit the ELDOR spectra.

The values of the fitting parameters that result in the best fit of the ELDOR spectra are given in Table 3. For each fitting parameter we were able to give a range of values that give a good fit of the ELDOR spectra, also reported in Table 3 in parentheses. The method of calculating this range is described in the SI. Examples of the best fits at two different detection frequencies are shown in Fig. 4. The agreement between best fit profiles and experimental data is rather good for all the samples and for all the detection frequencies. All the features present in the spectra appear at the correct position, though in some cases the intensities do not fully match.

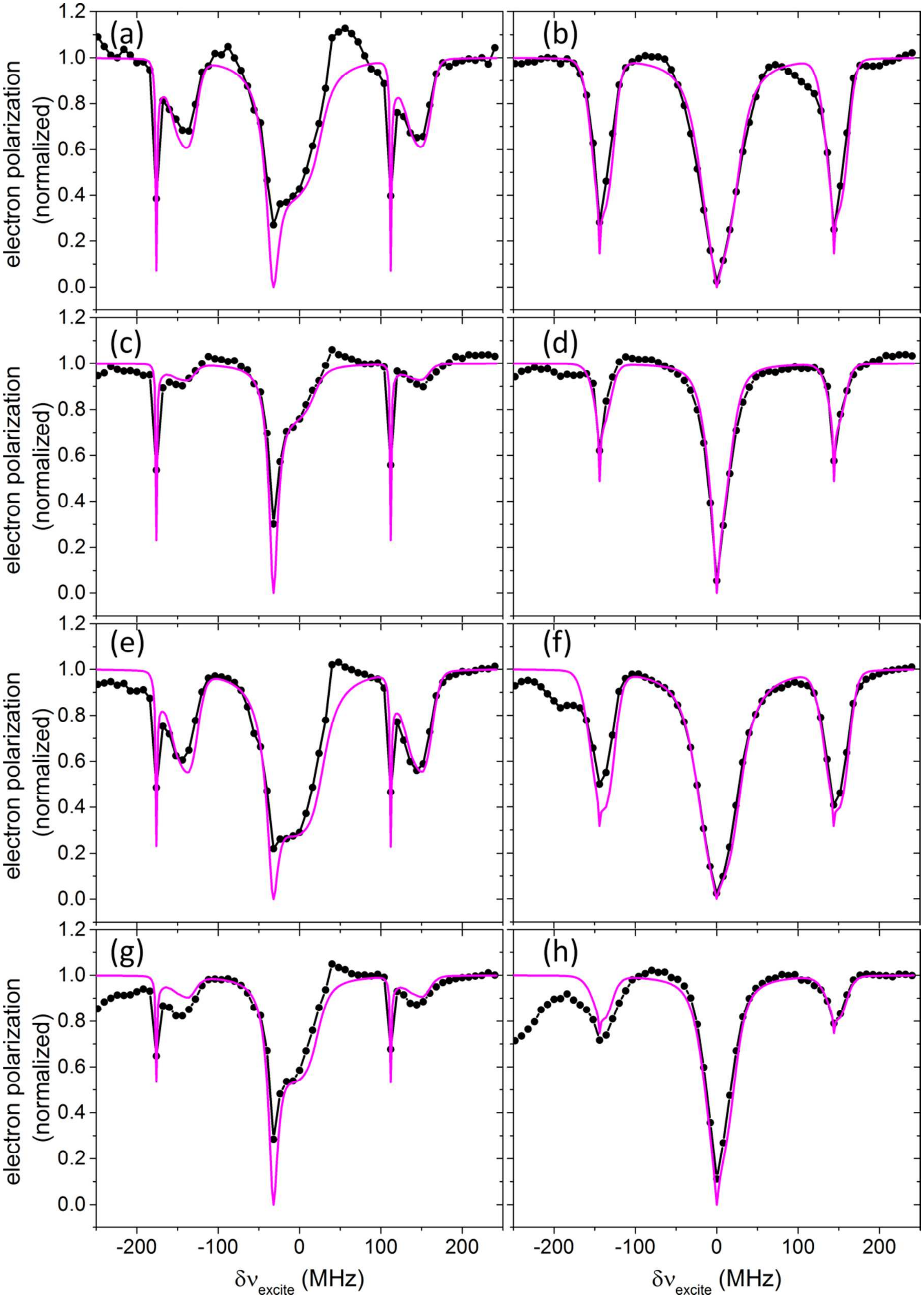

Figure 4. Best fit of the experimental ELDOR spectra (black symbols) with the model described in the text (magenta lines). The spectra here shown have been

acquired with detection frequencies of $\delta\nu_{detect}$ =-32 MHz (left panels) and $\delta\nu_{detect}$ =0 MHz (right panels). Each row is a different sample: (a, b) 5 mM, (c, d) 5 mM + Gd-DOTA, (e, f) 10 mM and (g, h) 10 mM + Gd-DOTA. The fits were calculated using the parameters listed in Table 3, and T_{1n} =300 sec, T=6.5 K, $\omega_1/2\pi$=600 kHz, t_{MW}=1 sec, the electron bin width set to 2 MHz, the electron spin concentration set to the OX063 concentration, and the proton concentration set to 100 M.

Sample	T_{1e} (ms)	$T_{\max}^{eSD}$ (ms)	Λ^{eSD} (μs^{-3})	T_{2e} (μs)	$\overline{A}^{\pm}$ (MHz)
5 mM OX063	500	0.278	0.23 (0.15-0.3)	600 (550-650)	0.055 (0.04-0.07)
5 mM OX063+ 1 mM Gd-DOTA	35	0.071	0.9 (0.7-1.1)	190 (133-250)	0.12 (0.09-0.14)
10 mM OX063	300	0.091	0.7 (0.6-0.8)	300 (250-350)	0.065 (0.05-0.08)
10 mM OX063 + 1 mM Gd-DOTA	25	0.021	3.1 (2.9-3.2)	75 (70-80)	0.155 (0.14-0.17)

Table 3. Most relevant parameters used to fit the ELDOR spectra; The best fit values as well as the acceptable ranges (in parenthesis) of Λ^{eSD} , $\overline{A}^{\pm}$ and T_{2e} are provided, along with the experimentally-measured T_{1e} and the $T_{\max}^{eSD}$ parameter derived from Λ^{eSD} . These ranges are determined via a fitting procedure of the ELDOR data described in the SI.

The best fit values of the spectral diffusion parameter Λ^{eSD} of the four samples differ from each other. The values of Λ^{eSD} are expected to depend on the bin size used in our model, thus we calculate the time constants $T_{\max}^{eSD}$ (Eq. 2) in order to give insight into the timescale of the eSD. First we notice a 2-3 fold difference in $T_{\max}^{eSD}$ between the 5 mM and 10 mM samples. This should be attributed to the increase in the OX063 concentration. Next we see a decrease in $T_{\max}^{eSD}$ after addition of the Gd(III) that could be attributed to the decrease of the T_{1e} value. The decrease of $T_{\max}^{eSD}$ when adding Gd(III) may also be due to the increase in the total electron spin concentration in the Gd samples. In fact, these samples exhibit a broad Gd-DOTA EPR line that partially overlaps with the trityl EPR line. It is important to note, though, that we do not observe direct DNP enhancement originating from the Gd-DOTA electron spins in the sample.[14]

To summarize, the analysis of the ELDOR spectra indicates that the three parameters Λ^{eSD}, $\overline{A}^{\pm}$ and T_{2e} change after the addition of Gd-DOTA. The main difference between the parameters of the 5 mM samples is a close to three-fold increase of Λ^{eSD} after the Gd-DOTA addition, which is may be a direct consequence of the ten-fold decrease of T_{1e}. For the 10 mM samples the Λ^{eSD} parameter again increases by about a factor of three, again presumably due to the about ten-fold change in T_{1e}. For these samples the $\overline{A}^{\pm}$ and T_{2e} parameters also change by around a factor of three. At this point we do not have an explanation for these changes.

Using the parameters in Table 3, $P_e(\delta\nu_{detect};\delta\nu_{excite})$ profiles can be evaluated and used to simulate DNP spectra.

Analysis of the DNP spectra

Fig. 5 shows the experimental DNP spectra measured at 6.5 K, rescaled such that the maximum enhancement of the 5 mM OX063 sample was equal to 1, exactly as in Fig. 3. The experimental spectra are overlaid with simulated spectra: the overall fit and the individual contributions of the SE and iCE contributions. The simulated spectra were obtained using the best fit k_{iCE} and k_{SE} coefficients according to Eq. 3, and were made up of the $S_{iCE}(\delta\nu_{MW})$ and $S_{SE}(\delta\nu_{MW})$ spectra, calculated according to Eqs. 4 and 5. $S_{iCE}(\delta\nu_{MW})$ and $S_{SE}(\delta\nu_{MW})$ were calculated using the EPR line and the electron polarization derived from the ELDOR spectra. The simulated spectra agree very well with the experimental ones, and the k_{iCE}/k_{SE} ratios hardly changed when Gd-DOTA was added (the k_{iCE} and k_{SE} coefficients are listed in Table 4). Consequently, it seems reasonable to conclude that the addition of Gd-DOTA increases both the SE and the iCE contributions to a similar extent. Note that the iCE shape also includes spectral features at ±144 MHz. These spectral features are due to contributions from ^{1}H, and are discussed in detail in Ref. [24]. The spectral features at ±100 MHz originating from radical clustering, will not be analyzed here.[24]

The $S_{iCE}(\delta\nu_{MW})$ and $S_{SE}(\delta\nu_{MW})$ basic spectra of the 5 mM and 10 mM samples without Gd-DOTA were normalized to one by choosing proper N_{iCE} and N_{SE} factors. The basic spectra of the samples with Gd-DOTA were normalized with the same N_{iCE} and N_{SE} factors, such that their intensity could be compared to the intensity of the spectra without Gd-DOTA. The ratios between maximum values of the basic spectra $S_{iCE,\max}^{+Gd}/S_{iCE,\max}$ and $S_{SE,\max}^{+Gd}/S_{SE,\max}$ were found to both be ~1.2 for the 5 mM and 10 mM samples, meaning that ~20% of the increase in the signal when adding Gd-DOTA can be attributed solely to the narrowing of the ELDOR spectra (less electron saturation). This is close to the ~30% experimental increase in the enhancement that was measured. It is however possible that some additional mechanisms also contribute to the increase in the enhancement (see below and SI).

When comparing the DNP spectra of the 5 mM and 10 mM samples, we note an increase in the enhancement as a consequence of the increase of the OX063 radical concentration, which causes an increase in the efficiency of the DNP processes.

In the literature there are reports showing that adding Gd(III) at 3.4 T and 1.4 K can increase the ^{13}C enhancement by a factor of 2 or even more,[14;15] much higher than the factor of 1.3 obtained in our study. Whether these values can be explained solely by the increase of the polarization gradients has yet to be seen. An example showing that it is possible to obtain a factor of two in nuclear enhancement by decreasing the T_{1e} in the ELDOR simulations is shown in the SI.

Moreover, it has been shown that at 6 T and 4 K, the addition of Gd(III) can also cause a decrease in nuclear enhancement.[18] In the framework of our findings, this decrease should be a result of the creation of very steep electron polarization gradients, due to quenching of the eSD by the shortening of T_{1e} through the addition of Gd(III).

Here we should mention that there is another mechanism reported in the literature[39;40] not connected to the electron depolarization of the EPR line, that also shows that shortening T_{1e} can lead to some increase in enhancement. This mechanism has to do with the ability of polarizing electrons to polarize the bulk nuclei around them. This increase in polarization can be explained by the increase in the DNP turnover rate when T_{1e} is decreased, i.e. the electron must recover quickly in order to effectively transfer its polarization to many nuclei. An example of this process is discussed in the SI, where we show that shortening T_{1e}, in a model system containing a single electron coupled to a two-dimensional grid of nuclei, results in a growth of the enhancement.

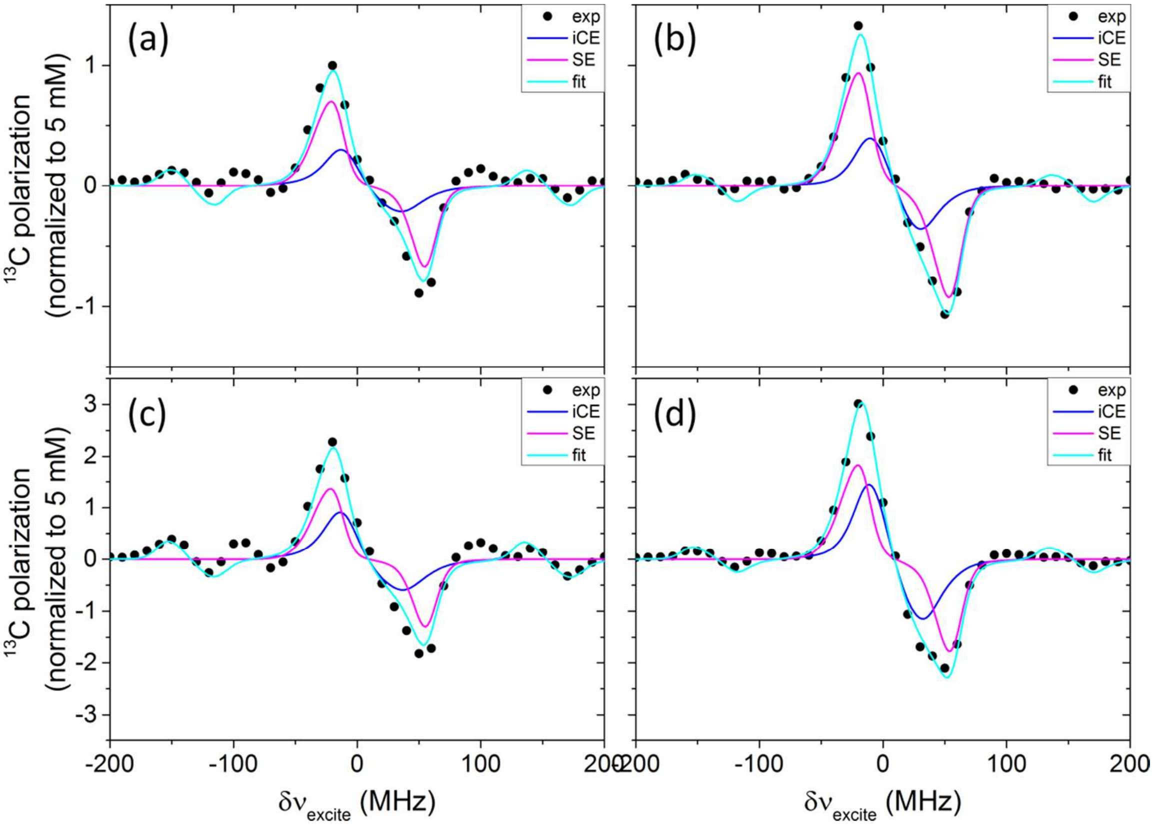

Figure 5. Best fit (cyan) of the experimental DNP spectra, obtained by summing the individual contributions of the SE (magenta) and iCE (blue) contributions. The panels are: (a) 5 mM, (b) 5 mM + Gd-DOTA, (c) 10 mM and (d) 10 mM + Gd-DOTA. The vertical axis in the figures are the ^{13}C signals measured as a function of $\delta\nu_{excite}$, where the signals are normalized with respect to the signal of the 5 mM sample (a).

Sample	k_{SE}	k_{iCE}	k_{SE}/k_{iCE}
5 mM OX063	0.7	0.3	2.3
5 mM OX063+ 1 mM Gd-DOTA	0.8	0.35	2.4

10 mM OX063	1.3	1.1	1.5
10 mM OX063 +1 mM Gd-DOTA	1.4	1.2	1.3

Table 4. Best fit weighting factors of the SE and iCE contributions, obtained from the analysis of the DNP spectra.

Conclusions:

In conclusion, we demonstrated that when the DNP spectra and the ELDOR spectra are analyzed simultaneously they can provide insight into the DNP mechanism. Our observations strengthen the notion that taking into account the electron polarization spread over the EPR spectrum due to eSD is necessary for the proper interpretation of the DNP data. It is important to remark that the present analysis also takes into account the fact that the electron depolarization is not only determined by the MW irradiation, the eSD mechanism and T_{1e}, but also by the SE-DNP mechanism. The analysis indicates that the relative iCE/SE contributions do not change much in the presence or in the absence of 1 mM Gd-DOTA, and that the increase in the overall DNP enhancements observed after addition of Gd-DOTA is a combined result of changes in T_{1e} and all three parameters: T_{2e}, Λ^{eSD}, $\bar{A}^{\pm}$. It is still unclear whether the mechanism responsible for changing the last two parameters depends on the changes in T_{1e} or not; this will become clearer after the same kind of analysis of ELDOR and DNP measurements will be conducted on a variety of additional systems.

It is helpful to think of the overall nuclear enhancement in the following manner: when we apply MW irradiation we are partially saturating most of the EPR spectrum; a large part of this saturation is due to eSD. The polarization gradient formed during MW irradiation is what determines the DNP enhancement. In this work we show that an increase in nuclear enhancement by adding Gd-DOTAREM is caused by a large polarization gradient across the EPR line. A 20% enhancement increase could be explained by the increase of this gradient manifested in a narrowing of the ELDOR spectra, though 20% is somewhat lower than what was experimentally observed. Thus, as shown in the SI, it is possible that the decrease in T_{1e}, increasing the turnover of electron polarization transfer to the nuclei, also contributes to the overall nuclear polarization.

More combined ELDOR-DNP experiments are necessary to estimate the relative contributions of the different processes, and to understand exactly how the different parameters in our ELDOR simulations affect the final DNP enhancement.

Acknowledgements:

We would like to thank Dr. Leah Casabianca for help with experiments early on in the project. This work was supported by the German-Israeli Project Co-operation of the DFG through a special allotment by the Ministry of Education and Research (BMBF) of the Federal Republic of Germany and partially by funds from the Spanish MINECO-FEDER to the University of Barcelona NMR ICTS, by

COST action TD1103 ‘‘Hyperpolarization Methods in NMR and MRI’’, FP7 ITN contract pNMR No. 317127, Ente Cassa di Risparmio di Firenze, MIUR PRIN 2012SK7ASN, and Instruct, part of the European Strategy Forum on Research Infrastructures (ESFRI). This research was also made possible in part by the historic generosity of the Harold Perlman Family. D.G. holds the Erich Klieger Professorial Chair in Chemical Physics.

Reference List

(1) A. W. Overhauser, *Phys.Rev.*, 1953, ***92***, 411-415.

(2) T. R. Carver and C. P. Slichter, *Phys.Rev.*, 1953, ***92***, 212-213.

(3) R. G. Griffin and T. F. Prisner, *Phys.Chem.Chem.Phys.*, 2010, ***12***, 5737-5740.

(4) J.-H. Ardenkjaer-Larsen, B. Fridlund, A. Gram, L. Hansson, M. H. Lerche, R. Servin, M. Thaning and K. Golman, *Proc.Natl.Acad.Sci.U.S.A*, 2003, ***100***, 10158-10163.

(5) J.-H. Ardenkjaer-Larsen, G. S. Boebinger, A. Comment, S. B. Duckett, A. S. Edison, F. Engelke, C. Griesinger, R. G. Griffin, C. Hilty, H. Maeda, G. Parigi, T. F. Prisner, E. Ravera, G. J. M. van Bentum, S. Vega, A. Webb, C. Luchinat, H. Schwalbe, and L. Frydman, *Angew.Chem.Int.Ed*, 2015, ***54***, 9162–9185.

(6) D. A. Hall, D. C. Maus, G. J. Gerfen, S. J. Inati, L. R. Becerra, F. W. Dahlquist and R. G. Griffin, *Science*, 1997, ***276***, 930-932.

(7) C. Laustsen, G. Pileio, M. C. D. Tayler, L. J. Brown, R. C. D. Brown, M. H. Levitt and J.-H. Ardenkjaer-Larsen, *Magn.Res.Med.*, 2012, ***68***, 1262-1265.

(8) G. D. Aquaro, F. Frijia, V. Positano, L. Menichetti, M. F. Santarelli, J. H. Ardenkjaer-Larsen, F. Wiesinger, V. Lionetti, S. L. Romano, G. Bianchi, D. Neglia, G. Giovannetti, R. F. Schulte, F. A. Recchia, L. Landini and M. Lombardi, *JACC.Cardiovasc.Imaging*, 2013, ***6***, 743-744.

(9) A. Flori, M. Liserani, S. Bowen, J. H. Ardenkjaer-Larsen and L. Menichetti, *J.Phys.Chem.A*, 2015, ***119***, 1885-1893.

(10) A. Flori, M. Liserani, F. Frijia, G. Giovannetti, V. Lionetti, V. Casieri, V. Positano, G. D. Aquaro, F. A. Recchia, M. F. Santarelli, L. Landini, J. H. Ardenkjaer-Larsen and L. Menichetti, *Contrast.Media Mol.Imaging*, 2015, ***10***, 194-202.

(11) T. Harris, G. Eliyahu, L. Frydman and H. Degani, *Proc.Natl.Acad.Sci.U.S.A*, 2009, ***106***, 18131-18136.

(12) T. Harris, H. Degani and L. Frydman, *NMR Biomed.*, 2013, ***26***, 1831-1843.

(13) A. Leftin, H. Degani and L. Frydman, *Am.J.Physiol Endocrinol.Metab*, 2013, ***305***, E1165-E1171.

(14) L. Lumata, M. E. Merritt, C. R. Malloy, A. D. Sherry and Z. Kovacs, *J.Phys.Chem.A*, 2012, ***116***, 5129-5138.

(15) J.-H. Ardenkjaer-Larsen, S. Macholl and H. Johannesson, *Appl.Magn.Reson.*, 2008, ***34***, 509-522.

(16) H. Johannesson, S. Macholl and J.-H. Ardenkjaer-Larsen, *J.Magn Reson.*, 2009, ***197***, 167-175.

(17) M. Batel, M. Krajewski, K. Weiss, O. With, A. Däpp, A. Hunkeler, M. Gimersky, K. P. Pruessmann, P. Boesiger, B. H. Meier, S. Kozerke and M. Ernst, *J.Magn.Reson.*, 2012, ***214***, 166-174.

(18) S. A. Walker, D. T. Edwards, T. A. Siaw, B. D. Armstrong and S. Han, *Phys.Chem.Chem.Phys.*, 2013, ***15***, 15106-15120.

(19) J. D. Jeffries, *Phys.Rev.*, 1957, ***106***, 164-165.

(20) C. F. Hwang and D. A. Hill, *Physical Review Letters*, 1967, ***19***, 1011-1014.

(21) B. N. Provotorov, *Sov.Phys.JETP*, 1962, ***14***, 1126-1131.

(22) Abragam, A.; Borghini, M. Dynamic Polarization of Nuclear Targets; In *Progress in Low Temperature Physics vol. 4*; Gorter, C. J., ed. North-Holland Publishing Company: Amsterdam, 1964; pp 384-449.

(23) M. Borghini, *Phys.Rev.Lett.*, 1968, ***20***, 419-421.

(24) D. Shimon, Y. Hovav, I. Kaminker, A. Feintuch, D. Goldfarb and S. Vega, *Phys.Chem.Chem.Phys.*, 2015, ***17***, 11868-11883.

(25) D. Banerjee, D. Shimon, A. Feintuch, S. Vega and D. Goldfarb, *J.Magn Reson.*, 2013, ***230***, 212-219.

(26) Y. Hovav, A. Feintuch and S. Vega, *J.Magn.Reson.*, 2010, ***207***, 176-189.

(27) Y. Hovav, A. Feintuch and S. Vega, *J.Magn.Reson.*, 2012, ***214***, 29-41.

(28) D. Shimon, Y. Hovav, A. Feintuch, D. Goldfarb and S. Vega, *Phys.Chem.Chem.Phys.*, 2012, ***14***, 5729-5743.

(29) Y. Hovav, A. Feintuch and S. Vega, *Phys.Chem.Chem.Phys.*, 2013, ***15***, 188-203.

(30) K. R. Thurber and R. Tycko, *J Chem Phys*, 2012, ***137***, 084508-084522.

(31) F. Mentink-Vigier, U. Akbey, Y. Hovav, S. Vega, H. Oschkinat and A. Feintuch, *J.Magn Reson.*, 2012, ***224***, 13-21.

(32) D. Mance, P. Gast, M. Huber, M. Baldus and K. L. Ivanov, *J.Chem.Phys.*, 2015, ***142***, 234201.

(33) B. Corzilius, V. K. Michaelis, S. Penzel, E. Ravera, A. Smith, C. Luchinat and R. G. Griffin, *J.Am.Chem.Soc.*, 2014, ***136***, 11716-11727.

(34) D. Shimon, A. Feintuch, D. Goldfarb and S. Vega, *Phys.Chem.Chem.Phys.*, 2014, ***16***, 6687-6699.

(35) T. V. Can, M. A. Caporini, F. Mentink-Vigier, B. Corzilius, J. J. Walish, M. Rosay, W. E. Maas, M. Baldus, S. Vega, T. M. Swager and R. G. Griffin, *J.Chem.Phys.*, 2014, ***141***, 064202.

(36) Y. Hovav, D. Shimon, I. Kaminker, A. Feintuch, D. Goldfarb and S. Vega, *Phys.Chem.Chem.Phys.*, 2015, ***17***, 6053-6065.

(37) S. C. Serra, A. Rosso and F. Tedoldi, *Phys.Chem.Chem.Phys.*, 2012, ***14***, 13299-13308.

(38) Y. Hovav, I. Kaminker, D. Shimon, A. Feintuch, D. Goldfarb and S. Vega, *Phys.Chem.Chem.Phys.*, 2015, ***17***, 226-244.

(39) K. N. Hu, G. T. Debelouchina, A. A. Smith and R. G. Griffin, *J.Chem.Phys.*, 2011, ***134***, 125105.

(40) V. K. Michaelis, A. A. Smith, B. Corzilius, O. Haze, T. M. Swager and R. G. Griffin, *J.Am.Chem.Soc.*, 2013, ***135***, 2935-2938.

(41) A. Feintuch, D. Shimon, Y. Hovav, D. Banerjee, I. Kaminker, Y. Lipkin, K. Zibzener, B. Epel, S. Vega and D. Goldfarb, *J.Magn Reson.*, 2011, ***209***, 136-141.

(42) Y. Hovav, A. Feintuch and S. Vega, *J.Chem.Phys.*, 2011, ***134***, 074509.

(43) H. Jäger, A. Koch, V. Maus, H. W. Spiess and G. Jeschke, *J.Magn.Reson.*, 2008, ***194***, 254-263.

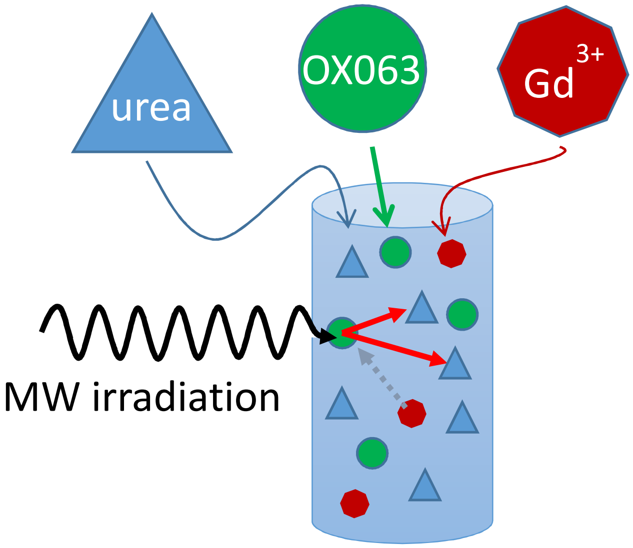
urea
OX063
Gd^{3+}
MW irradiation